AD-A147 406 CALCULATIONS OF HIGH-CURRENT CHARACTERISTICS OF SILICON DIODES AT MICROWAVE FREQUENCIES(U) HARRY DIAMOND LABS ADELPHI MD A L WARD OCT 84 HDL-TR-2057 1/1

UNCLASSIFIED F/G 9/1 NL

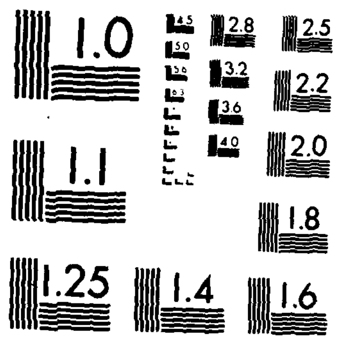

MICROCOPY RESOLUTION TEST CHART
NATIONAL BUREAU OF STANDARDS-1963-A

UNCLASSIFIED

SECURITY CLASSIFICATION OF THIS PAGE (When Data Entered)

REPORT DOCUMENTATION PAGE

READ INSTRUCTIONS BEFORE COMPLETING FORM

1. REPORT NUMBER HDL-TR-2057	2. GOVT ACCESSION NO. AD-A147406	3. RECIPIENT'S CATALOG NUMBER
4. TITLE (and Subtitle) Calculations of High-Current Characteristics of Silicon Diodes at Microwave Frequencies		5. TYPE OF REPORT & PERIOD COVERED Technical Report
		6. PERFORMING ORG. REPORT NUMBER
7. AUTHOR(s) Alford L. Ward		8. CONTRACT OR GRANT NUMBER(s)
9. PERFORMING ORGANIZATION NAME AND ADDRESS Harry Diamond Laboratories 2800 Powder Mill Road Adelphi, MD 20783-1197		10. PROGRAM ELEMENT, PROJECT, TASK AREA & WORK UNIT NUMBERS Program Ele: 62120A DA Project: 1L162120AH25
11. CONTROLLING OFFICE NAME AND ADDRESS U.S. Army Materiel Command 5001 Eisenhower Ave Alexandria, VA 22333-0001		12. REPORT DATE October 1984
		13. NUMBER OF PAGES 25
14. MONITORING AGENCY NAME & ADDRESS(if different from Controlling Office)		15. SECURITY CLASS. (of this report) UNCLASSIFIED
		15a. DECLASSIFICATION/DOWNGRADING SCHEDULE

16. DISTRIBUTION STATEMENT (of this Report)

Approved for public release; distribution unlimited.

17. DISTRIBUTION STATEMENT (of the abstract entered in Block 20, if different from Report)

18. SUPPLEMENTARY NOTES

HDL Project: E013E1

AMS Code: 612120H25001

19. KEY WORDS (Continue on reverse side if necessary and identify by block number)

Silicon diode

Microwave frequency

Second breakdown

Forward conduction

Avalanche multiplication

20. ABSTRACT (Continue on reverse side if necessary and identify by block number)

Dynamic current/voltage characteristics are calculated for silicon diodes at microwave frequencies. Forward and reverse half cycles are studied separately. Little current flows unless the forward half period exceeds the carrier transit time; then, as the frequency decreases, the peak forward current increases essentially linearly with the half period, until the dc value is attained. Avalanche multiplication is noted in the forward direction at about one half of the reverse breakdown voltage. Below the reverse breakdown voltage, the current consists solely of the stored forward charge. Above the reverse breakdown voltage, the peak current has a maximum at a frequency which depends on the diode width and temperature.

DD FORM 1473, 1 JAN 73 EDITION OF 1 NOV 65 IS OBSOLETE

UNCLASSIFIED

 SECURITY CLASSIFICATION OF THIS PAGE (When Data Entered)

CONTENTS

Page

1. INTRODUCTION 5

2. COMPUTER PROGRAM 6

3. FORWARD HALF CYCLE 7

4. REVERSE HALF CYCLE 9

5. REVERSE AVALANCHING 10

6. FORWARD AVALANCHING 13

7. TEMPERATURE DEPENDENCE 14

8. CONCLUSION 18

LITERATURE CITED 19

DISTRIBUTION 21

FIGURES

1. External circuit used in calculations 7

2. Forward current/voltage characteristics for 1-μm p-i-n diode for constant voltage and various frequencies 8

3. Peak forward current density as a function of applied frequency for various diode widths and voltages 9

4. Current, voltage, and power during forward and reverse half cycles with an applied voltage of 60 V peak on a 4-μm diode 10

5. Maximum current density as a function of frequency for reverse-bias (half-cycle) 0.2-μm diode 11

6. Dynamic current/voltage reverse characteristics for 100-V peak applied voltage 11

7. Overvoltage as a function of rate of voltage rise for data for figure 5 12

8. Comparison of forward and reverse current peaks as a function of frequency for 0.2-μm diode 12

9. Forward turn-on transients for 100-V maximum applied voltage at 160 GHz 13

FIGURES (Cont'd)

Page

10. Charge distributions for turn-on transient of figure 9 14

11. Field distributions for transient of figure 9 14

12. Maximum current densities as a function of frequency at specified temperatures 15

13. Effect of thermal injection currents (J_o) upon maximum current densities 15

14. Maximum current densities as a function of frequency at labeled temperatures 16

15. Reverse current density and voltage as a function of time for a 1-μm diode at 4.8 GHz 17

16. Average diode temperature and rate of temperature rise as a function of time 17

17. Distribution of temperature across diode at specified times 17

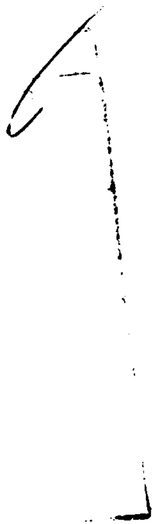

1. INTRODUCTION

Second breakdown due to a sinusoidal voltage waveform is of interest to the electrical-overstress/electostatic-discharge community as well as to the microwave and electromagnetic radiation communities. By far the majority of second-breakdown studies have been for single-polarity square pulses. Square-pulse studies are convenient for both the experimentalist and the theoretician. Several investigators have predicted second breakdown due to sinusoidal waveforms using suitable modification of square-pulse data.

Whalen and Domingos[1] have compared square- and rf-pulse overstress data for bipolar uhf transistors. They reported that the pulse energy required to cause failure is lowest for reverse-polarity square pulses, intermediate for rf pulses (240 MHz), and highest for forward-polarity square pulses. Their finding that intermediate energy causes failure for rf pulses is logical in the thermal model of second breakdown, even though the thermal model itself does not distinguish between forward and reverse breakdown. Again, the thermal model is inadequate to study the frequency dependence of rf-pulse second breakdown. In general, the thermal model is valid for breakdown times greater than the thermal time constant of the device, usually on the order of a microsecond. For shorter breakdown times, the electrical characteristics dominate; this regime has usually been called the current-mode[2] second breakdown. Greater frequency dependence of rf-pulse second breakdown should be expected in the current-mode time regime.

The calculations reported herein were made with the Harry Diamond Laboratories (HDL) DIODE computer program that has been used successfully to calculate second breakdown[3] in reverse-bias junctions and to study various modes of avalanche oscillations[4] (IMPATT, TRAPATT, MULTIPATT*). The most important limitations of the present program are (1) it is limited to one-dimensional calculations, (2) it neglects thermal conduction, and (3) it is limited to one polarity in a given calculation.

Rf damage of a semiconductor junction is caused by the temperature rise in the high-field junction area. The disparity of the electronic time scale (dielectric time constant of the order of picoseconds) and the thermal time

---

[1] *J. J. Whalen and H. Domingos, Square Pulse and RF Pulse Overstressing of UHF Transistors, Proceedings of the Electrical Overstress/Electrostatic Discharge Symposium, EOS-1 (1979), 140-146.*

[2] *J. H. Yee, W. J. Orvis, L. C. Martin, and J. C. Peterson, Modeling of Current and Thermal Mode Second Breakdown Phenomena, Proceedings of the Electrical Overstress/Electrostatic Discharge Symposium, EOS-4 (1982), 76-81.*

[3] *A. L. Ward, Calculations of Second Breakdown in Silicon, Harry Diamond Laboratories, HDL-TR-1978 (August 1982).*

[4] *A. L. Ward, Modes of Avalanche Oscillations in Silicon Diodes, IEEE Trans. Electron Devices, ED-25 (1978), 683-687.*

**IMPATT--impact avalanche transit time; TRAPATT--trapped plasma avalanche transit time; MULTIPATT--multiple avalanche transit time.*

constant (on the order of microseconds) prevents the calculation (at a reasonable computer cost) of a sufficient temperature rise to cause damage. However, the rate of temperature rise may be calculated at selected temperatures; then the time required to reach the damage temperature may be approximated. Damage may be the result of thermal displacement of dopant atoms and/or the melting of channels.

This investigation studies the basic dynamic characteristics of silicon junction diodes upon application of a high-power rf pulse. The next section describes the computer program. The forward half cycle and the reverse half cycle are treated separately in the following sections.

2. COMPUTER PROGRAM

A computer program that has been used to study square-pulse second breakdown in silicon diodes[3] has now been used to study the microwave characteristics of silicon diodes.

The computer program was designed to study only reverse-bias breakdown, but it can be used to study large forward-bias current when the diffusion component of the current is small compared to the conduction component.[5] Negative fields tend to lead to calculation instability; therefore, the forward and reverse half cycles of the microwave signal must be calculated separately. The charge distributions at the end of the forward half cycle are used as initial conditions for the reverse half cycle. Space-charge-free conditions (i.e., when the mobile charges equal the fixed charges) are used as initial conditions for the forward half cycle.

The circuit simulated is usually chosen to consist of a small capacitance shunting the diode, with the voltage applied through a series resistance. This circuit is shown in figure 1. The applied voltage may be chosen to be constant, to have an incremental step voltage, or to have the applied sinusoidal half wave used mainly in this study. The initial voltage need not be set equal to the applied voltage. Among other available external circuits is one with an inductance in series with the external resistance. Calculations may be made at a constant temperature, or the temperature can be calculated to increase due to the local power density. Results reported in sections 3 through 6 are for room-temperature calculations; temperature effects are considered in section 7.

---

[3] *A. L. Ward, Calculations of Second Breakdown in Silicon, Harry Diamond Laboratories, HDL-TR-1978 (August 1982).*

[5] *A. L. Ward, Oscillating Voltage Pulses and Second Breakdown, Proceedings of the Electrical Overstress/Electrostatic Discharge Symposium, EOS-2 (1980), 130-139.*

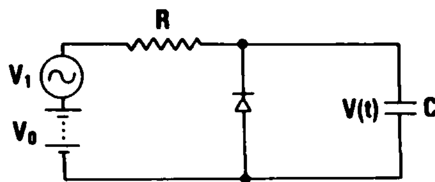

Figure 1. External circuit used in calculations.

3. FORWARD HALF CYCLE

We first discuss calculations of the characteristics of the forward-bias half cycle of diodes subject to an applied microwave voltage. Figure 2 shows calculations for a 1-μm silicon p-i-n diode. The series resistance is 50 Ω, the shunt capacitance is 0.2 pF, and the area is 1×10^{-6} cm^2. The low-level recombination lifetime is 50 μs in the intrinsic material; the effective lifetime decreases as the current increases. Figure 2(a) shows the current density as a function of time for four applied frequencies; also shown is the turn-on transient for a fixed voltage. The carrier transit time across a 1-μm diode at saturated carrier velocities is 10 ps. Examples of charge and field distributions during a turn-on pulse may be found in section 6. Figure 2(a) shows that four or five transit times are required for the peak microwave current pulse to approach the constant-voltage saturation current.

Figure 2(b) shows the diode voltage as a function of time for the same applied voltage. Note that the voltage peaks for the constant applied voltage case. The decrease in diode voltage is due to the current flow in the series resistance. The voltage drop is greater for large diode areas or for large series resistances. The peaking of the voltage during the turn-on transient has been observed in our laboratories and by others. The current/voltage characteristics for the various frequencies are shown in figure 2(c). The counterclockwise current/voltage excursion indicates the diode's inductive reactance, a result of the time required for the current to increase.

The current-density maxima are plotted as a function of frequency in figure 3 for the 1-μm p-i-n diode at two applied voltages. Also shown are similar plots for 4-, 20-, and 100-μm diodes.

The probable usage of diodes of these various widths can be determined by the reverse-breakdown voltage. The breakdown voltage, V_B, as a function of diode width for silicon diodes which are just punched through at first breakdown, is given by[3]

$$V_B = 21d^{0.86} ,$$

where the diode width, d, is given in micrometers. For example, 1-μm diodes have a reverse breakdown of about 21 V while 100-μm diodes break down at about 1100 V. The cutoff frequencies shown in figure 3 are the upper frequencies usable for each diode width.

---

[3] *A. L. Ward, Calculations of Second Breakdown in Silicon, Harry Diamond Laboratories, HDL-TR-1978 (August 1982).*

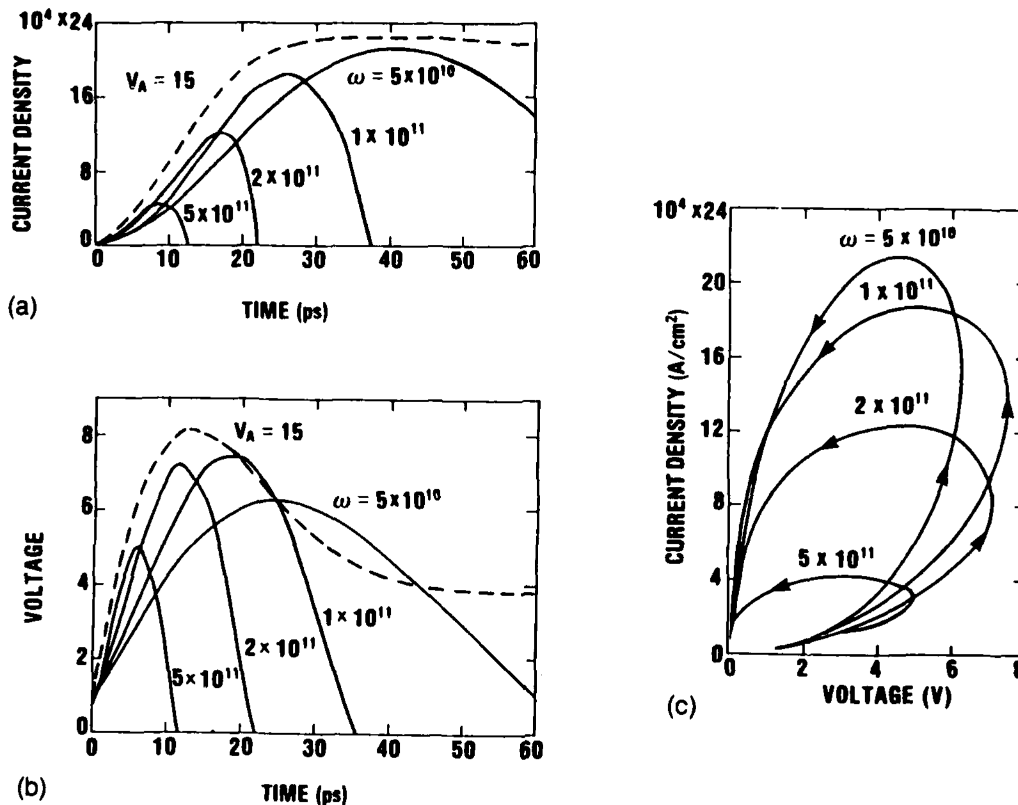

Figure 2. Forward current/voltage characteristics for 1-μm p-i-n diode for constant voltage and various frequencies: (a) current density as a function of time, (b) voltage as a function of time, and (c) current density as a function of voltage.

The 4-μm diode of figure 3 is N-type, doped to 5×10^{15} cm^{-3}, whereas the others are p-i-n diodes. Past experience has shown that doping level has little effect on the diode forward characteristics at the high current levels considered here. The dc current levels at the same applied voltage are indicated at the left margin of the figure. The maximum frequency shown for each diode is approximately the inverse of the transit time (at saturated velocity) for each device. It may be noted that more transit times are required for current saturation for the longer diodes. With this in mind, we find that our calculations seem compatible with the measurements of Caulton et al.[6] They measured voltage waveforms for diodes of about 100 to 300 μm and observed compression of the voltage waveform due to forward current flow. One diode of unspecified thickness showed no compression above 41 MHz, but sharp compression at lower frequencies. They found that this frequency increased for decreased diode thickness, in agreement with our calculations.

---

[6] *M. Caulton, A. Rosen, P. J. Stabile, and A. Gombar, p-i-n Diodes for Low-Frequency High-Power Switching Applications, IEEE Trans. Microwave Theory Tech.,* <u>*MTT-30*</u> *(1982), 875-882.*

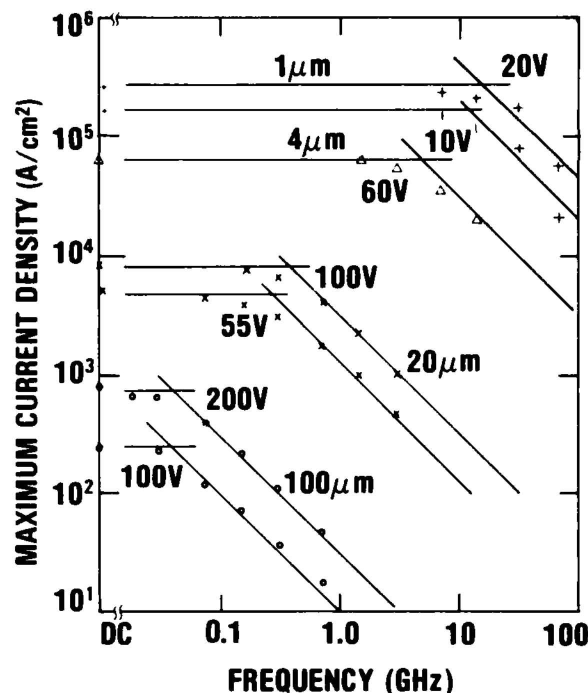

Figure 3. Peak forward current density as a function of applied frequency for various diode widths and voltages. Diagonal lines are drawn with slope of -1.

4. REVERSE HALF CYCLE

As stated earlier, the mobile charge distributions at the end of the forward-bias pulse are used as initial conditions for the reverse-bias pulse. The two calculations are then matched at the zero voltage point of the applied voltage waveform. This entails minor extrapolations of the calculated diode voltage and current toward the crossing point. The diode current is zero for zero diode voltage since only the conduction current is plotted. Diffusion and displacement currents are calculated but are not plotted here. Figure 4 shows the composite waveform for a 4-μm N-type diode doped to 5×10^{15} cm^{-3}. The maximum applied voltage is 60 V for each bias direction. The series resistance is again 50 Ω, the shunt capacitance is 0.4 pF, and the area is 1×10^{-5} cm^2. The voltage compression in the forward half cycle is about 1/3, as compared to the reverse half cycle. As noted earlier, this depends on the diode area used as well as the series resistance.

The calculated power dissipated is also shown in figure 4. Note that little power is dissipated in the reverse half cycle compared to the forward half cycle. This changes drastically when the reverse-breakdown voltage is exceeded. The shoulder on the current decay (at about 250 ps) is due to the transition from space-charge-limited to space-charge-free conditions.[5]

[5] *A. L. Ward, Oscillating Voltage Pulses and Second Breakdown, Proceedings of the Electrical Overstress/Electrostatic Discharge Symposium,* *EOS-2* *(1980), 130-139.*

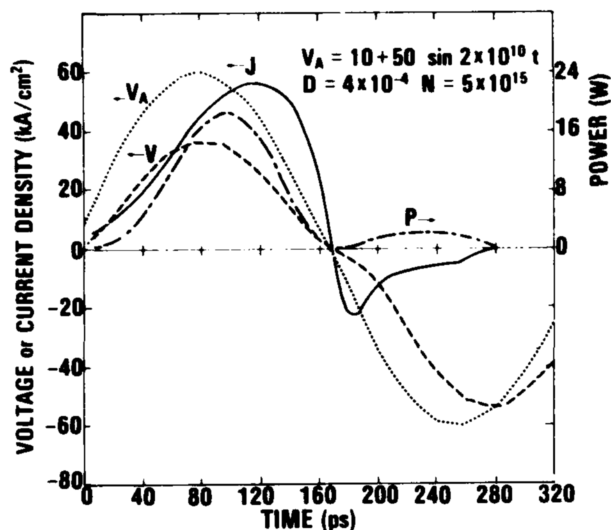

Figure 4. Current, voltage, and power during forward and reverse half cycles with an applied voltage of 60 V peak on a 4-μm diode.

5. REVERSE AVALANCHING

The reverse current may exceed the forward current when the avalanche voltage is exceeded. Maximum current densities calculated as a function of frequency are shown in figure 5 for a 0.2-μm p-i-n diode. This diode has an avalanche breakdown voltage of 11 V; narrower diodes will have field-emission-assisted breakdown (not calculable with the present program). The dropoff of the current peak at high frequencies was expected (but not the sharpness), although that at lower frequencies was not. The maximum current shown for an applied voltage of 100 V at the lowest frequency is lower than that shown for the same dc voltage, because only the initial peak of a relaxation oscillation[4] is shown. Assuming an area of 1×10^{-6} cm^2, appropriate for this diode, a maximum instantaneous power of over 1000 W is dissipated for the highest applied voltage. This heat is generated in a volume of 2×10^{-11} cm^3, so that the power density is 5×10^{13} W/cm^3 and the temperature rise exceeds 1 K per picosecond. This rate of rise depends only on the current density and the electric field and is thus independent of the area chosen. If the current were constant at the peak current, the diode would burn out in about 1 ns, making an experimental measurement of pulse-length dependence very difficult. The dashed curve for 200 V applied is calculated with a shunt capacitance of 0.1 pF, and the others with 0.2 pF.

The dropoff of the peak current as the frequency decreases may be understood with the aid of figure 6, where the current/voltage dynamic characteristics are shown for 100 V applied. An area of 1×10^{-6} cm^2 is assumed. The characteristics are traversed in a counterclockwise direction with time. This is a result of the inductive effect of carrier transport. Figure 6 shows that the breakdown (maximum) voltage increases with frequency, and the current peak increases with the voltage peak.

---

[4]*A. L. Ward, Modes of Avalanche Oscillations in Silicon Diodes, IEEE Trans. Electron Devices,* <u>*ED-25*</u> *(1978), 683-687.*

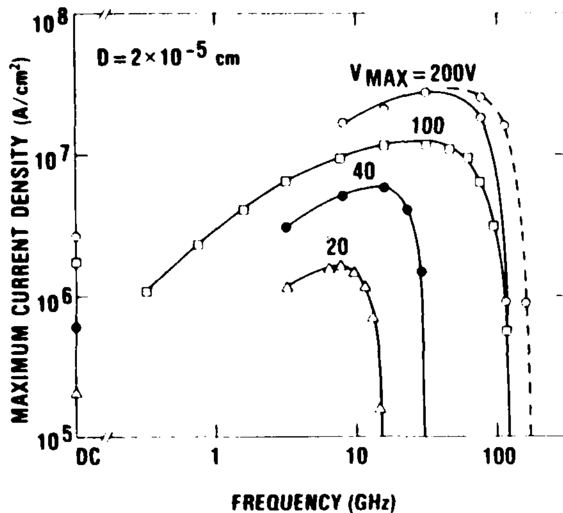

Figure 5. Maximum current density as a function of frequency for reverse-bias (half-cycle) 0.2-μm diode. Parameter is peak applied voltage.

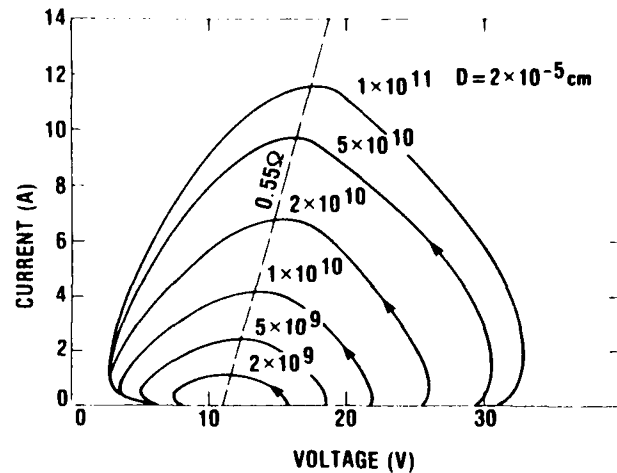

Figure 6. Dynamic current/voltage reverse characteristics for 100-V peak applied voltage. Parameter is angular frequency, $\omega = 2\pi f$.

Earlier calculations[3] have shown that second-breakdown overvoltages increase to the 2/3 power of the rate of rise of the applied voltage. Figure 7 is a plot of the over-voltage as a function of the rate of voltage rise for the characteristics of figure 6. A straight line results on this log-log plot when a breakdown of 11 V is assumed; deviations result from assumed breakdown voltages of 10 or 12 V. This breakdown voltage agrees with that found in figure 6 when the current peaks are extrapolated to zero current. The static characteristic indicates a differential resistance of 0.55 Ω. This is less than the forward differential resistance in the same current range and may be correlated with the lower power for second breakdown in the reverse- as compared to the forward-bias direction. Further calculations will be required to determine whether the slope of 0.58 seen in figure 6 applies generally to first-breakdown voltage as compared to the slope of 0.67 for second breakdown.

Comparisons of forward and reverse current peaks as a function of frequency are shown in figure 8 at two applied voltages. The sharp high-frequency cutoff of the reverse-bias current peak is contrasted with the nearly linear dropoff of the forward current peak. The slight current peak for the forward-bias maximum currents results from a large voltage overshoot in the turn-on transient. The unfilled triangle points of the reverse-bias curves were calculated with initial space-charge-free conditions; the filled-in circle points were calculated with stored charge resulting from a preceding forward

[3] *A. L. Ward, Calculations of Second Breakdown in Silicon, Harry Diamond Laboratories, HDL-TR-1978 (August 1982).*

half cycle. As shown previously,[5] stored charges generally reduce breakdown voltages and currents. The exceptional point at the highest frequency may be due to the fact that the same stored charge was assumed for the initial conditions for all frequencies.

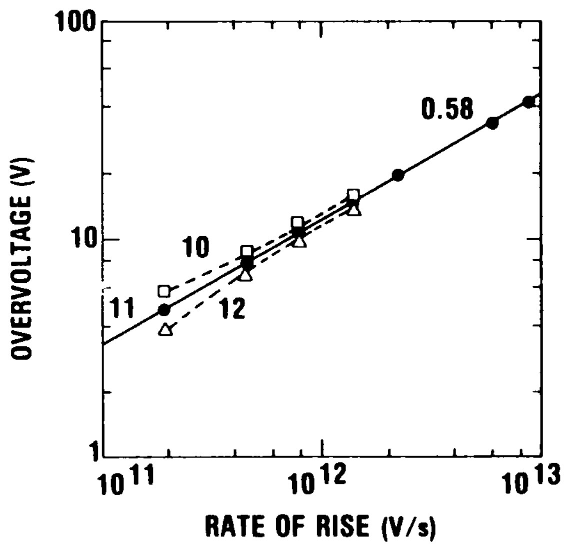

Figure 7. Overvoltage as a function of rate of voltage rise for data for figure 5. Assumed breakdown voltages are 10, 11, or 12 V. Slope of straight line is 0.58.

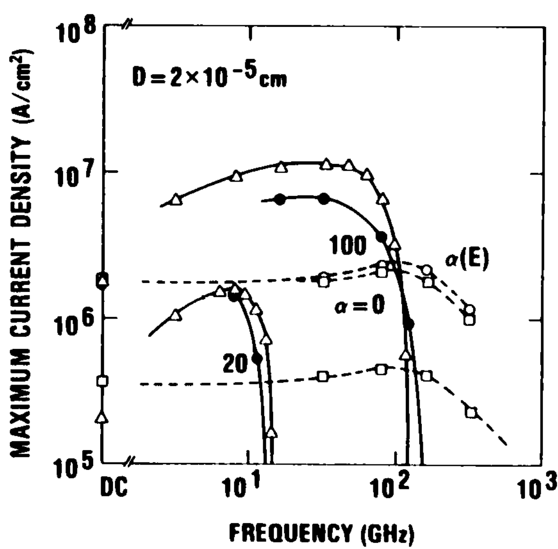

Figure 8. Comparison of forward and reverse current peaks as a function of frequency for 0.2-μm diode. Parameter is maximum applied voltage. Empty circles and squares are for forward bias, with and without avalanching, respectively. Filled circles and triangles indicate reverse bias with and without stored charges, respectively.

[5] *A. L. Ward, Oscillating Voltage Pulses and Second Breakdown, Proceedings of the Electrical Overstress/Electrostatic Discharge Symposium,* *EOS-2* *(1980), 130-139.*

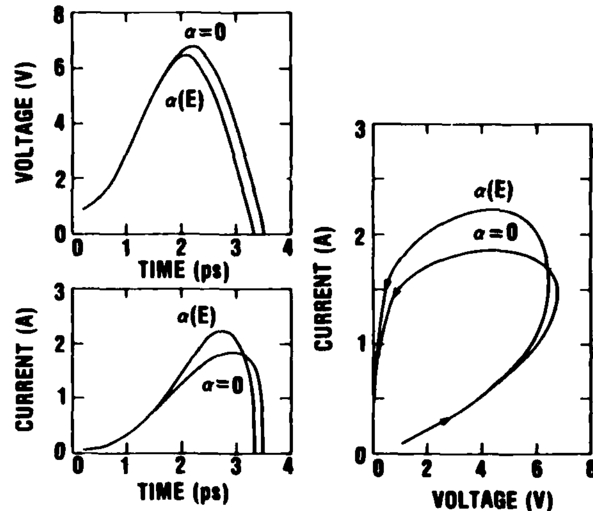

Figure 9. Forward turn-on transients for 100-V maximum applied voltage at 160 GHz. Curves are labeled for inclusion or exclusion of avalanching.

6. FORWARD AVALANCHING

Avalanching will also occur in forward-biased diodes[5] with sufficient applied voltages. This is shown for the 100-V forward-bias curves in figure 8. No difference is found in dc calculations with or without avalanche multiplication since the steady-state voltage is too low. Comparisons of current and voltage forward transients at 160 GHz are shown in figure 9. An increase in current due to avalanching is evident at about 5 or 6 V; this is just about half the reverse-bias avalanche breakdown of 11 V. This ratio is typical of many calculations and results from the high forward (unmultiplied) current.

The turn-on transient of the avalanching forward-current pulse of figure 9 is shown in figure 10. The solid curves show the doping profile of the p-i-n diode. Electrons (wide-dashed curves) move to the right, and holes (narrow-dashed curves) move to the left. At the saturation velocity, carriers move 100 nm (0.1 μm) in 1 ps. For reasons of clarity, charge distributions during the current decay are not shown in figure 10. In this case the current decay is so rapid that little charge redistribution can occur. Since the total current must be constant in space across the diode, displacement current must flow in the region devoid of enough carriers to provide sufficient conduction current. The result is that the field increases initially in the center of the diode. Field distributions during the turn-on transient of figure 10 are shown in figure 11. Avalanching occurs at fields about 4×10^5 V/cm, as may be seen from figures 9 and 11. This is about one-half the reverse-bias breakdown field for this diode.

---

[5] *A. L. Ward, Oscillating Voltage Pulses and Second Breakdown, Proceedings of the Electrical Overstress/Electrostatic Discharge Symposium, EOS-2 (1980), 130-139.*

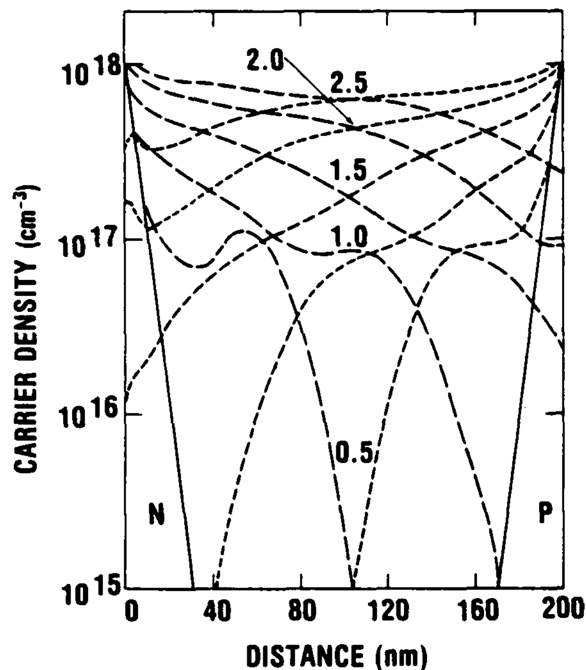

Figure 10. Charge distributions for turn-on transient of figure 9. Parameter is time in picoseconds.

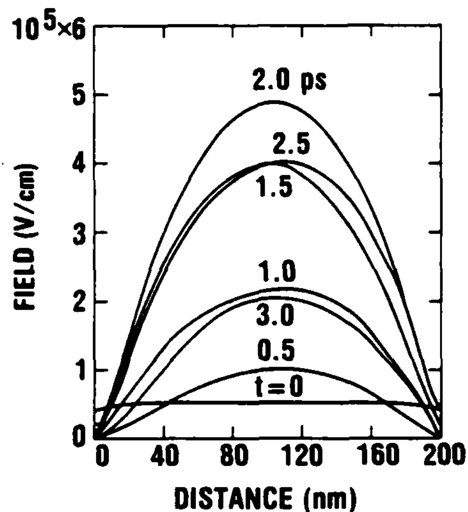

Figure 11. Field distributions for transient of figure 9. Parameter is time in picoseconds.

7. TEMPERATURE DEPENDENCE

Calculations have also been made of microwave characteristics at higher temperatures. It is not feasible to make computer runs long enough to obtain temperatures even approaching burnout temperatures, so constant-temperature calculations have been made at various higher temperatures. For the forward half cycle, the high-frequency cutoff shifts to lower frequencies at higher temperatures, because of the reduction of mobility and saturation velocity with temperature increase. This reduced cutoff frequency is shown in figure 12 for a p-i-n diode of 1-μm width; the peak applied voltage is 100 V. At lower frequency there is also an increase in the forward current (not shown) with temperature, because of a reduction of the recombination rate. This, in turn, results from the increase of the intrinsic carrier density with temperature.

In the reverse half cycle the temperature dependence results from the variation of the avalanche coefficients as well as the saturation velocity with temperature. The maximum current densities for reverse conduction for the 1-μm p-i-n diode at various temperatures are also shown in figure 12. The reduction in peak currents with increasing temperature is quite large, partially because of the decrease in cutoff frequency (a saturation velocity effect) and partially because of the decrease in the avalanche coefficients with temperature. The highest temperature curve shows a less sharp high-frequency cutoff than the others. This gradual cutoff results from the as-

sumption that the thermal injection current[3] was the equilibrium value for the indicated temperature. For applied pulse lengths less than the diode thermal time constant (of the order of a microsecond), there is little heat conducted and the thermal injection current should correspond to a lower temperature. Figure 13 shows the results for calculations made with thermal injection currents corresponding to the 100 and 200 K less than the bulk temperature. Lower injection currents lower the cutoff frequency but increase the current maxima at lower frequencies.

Further calculations of the temperature dependence of microwave current peaks were made for voltage peaks of 60 V applied to the same diode. A second difference in parameters was chosen to illustrate the effect of diode area upon the current peaks. In figure 14 the area was chosen to be 1×10^{-6} cm^2, rather than the 1×10^{-5} cm^2 used in figure 12. The series resistance was 50 Ω and the shunt capacitance was 0.2 pF in both cases. A comparison of figures 12 and 14 shows that the peak current-density maxima for the smaller area diode are greater than for the larger area diode, even though the applied voltage is less (see fig. 5 for the variation of current maxima with applied voltage).

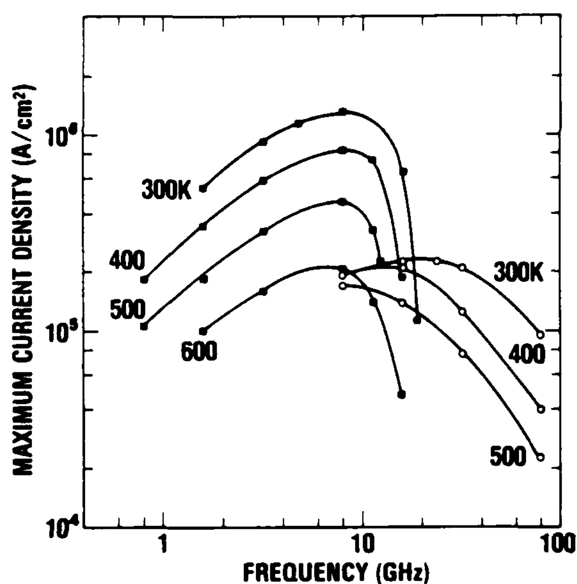

Figure 12. Maximum current densities as a function of frequency at specified temperatures. Forward-bias data are shown as open circles and reverse-bias data as filled squares.

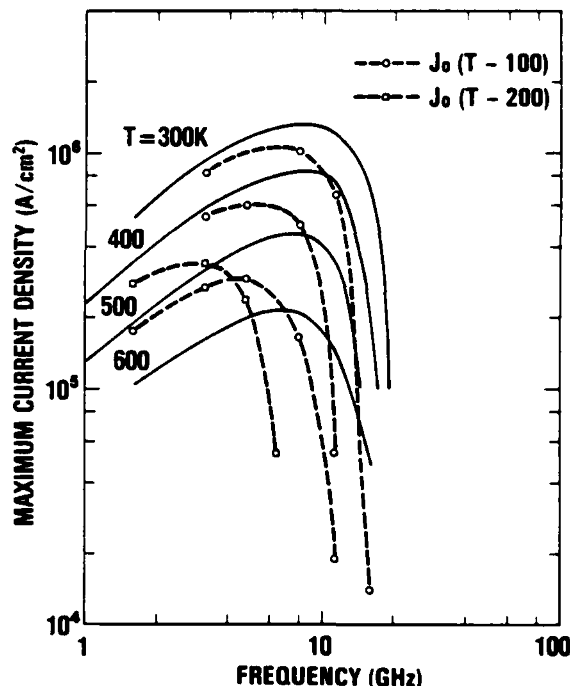

Figure 13. Effect of thermal injection currents (J_o) upon maximum current densities. Solid lines without points are fully isothermal data of figure 12.

---

[3] *A. L. Ward, Calculations of Second Breakdown in Silicon, Harry Diamond Laboratories, HDL-TR-1978 (August 1982).*

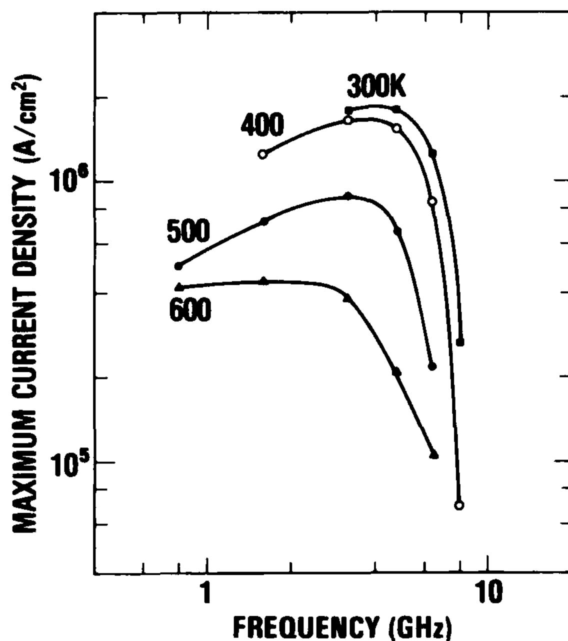

Figure 14. Maximum current densities as a function of frequency at labeled temperatures. Maximum of voltage is 60 V and diode area is 1×10^{-6} cm^2.

Higher transient current-density peaks for smaller area diodes result from the reduced voltage drop in the external resistor. This follows from the lower total diode current (current density times area) and consequently a higher voltage across the diode. The lower cutoff frequency shown in figure 14 compared to figure 12 is a result of the lower applied voltage (compare fig. 5). There is little difference in the 300 and 400 K curves in figure 14; this is because the higher breakdown voltage at 400 K results in higher current peaks (compare fig. 6), partially offsetting the reduced ionization coefficient and saturation velocity.

Although the initial temperature was assumed constant across the diode, calculations were also made with the option for the temperature to increase due to power being dissipated in the diode. Figure 15 shows the diode voltage and current density as a function of time for one point (4.8 GHz) on the 300 K curve of figure 14. The breakdown voltage of this diode is extrapolated to be 40 V. The maximum dissipated power during the pulse is just under 80 W, and the average over the reverse half cycle is about 5 W. Figure 16 shows the average diode temperature as a function of time for this simulation. Although the increase in average temperature is just over 3 K for this cycle, the maximum rate of temperature rise at the current peak is 450 K per nanosecond. The average rate over the entire cycle is about 15 K per nanosecond. The distribution of temperature across the diode at selected times is shown in figure 17, which shows that the temperature peaks at or near each end of the diode. These peaks are a result of the high space-charge-induced electric fields in these regions. In reality, the fields and temperatures should drop sharply from the peak at each boundary. Their failure to do so resulted from too-low doping levels assumed for these regions. These lower doping levels were used to allow calculations to be made at lower currents and at lower costs.

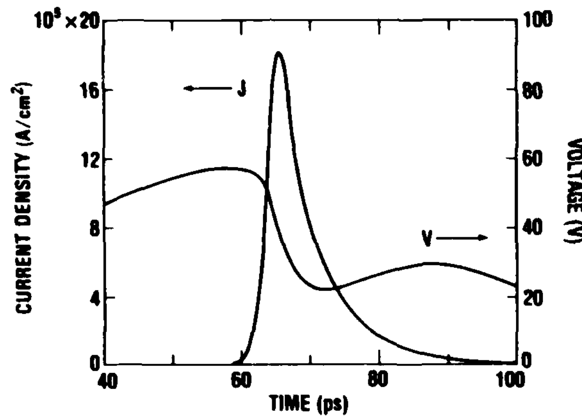

Figure 15. Reverse current density and voltage as a function of time for a 1-μm diode at 4.8 GHz.

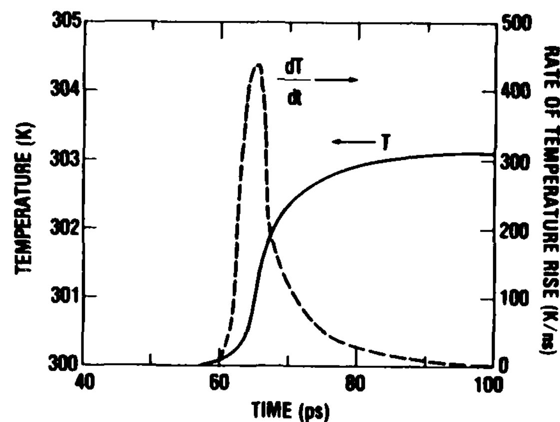

Figure 16. Average diode temperature and rate of temperature rise as a function of time.

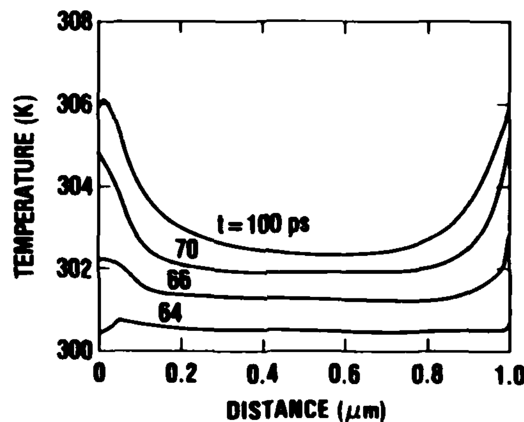

Figure 17. Distribution of temperature across diode at specified times.

The temperature distribution during the forward half cycle has a peak in the center of the intrinsic region. The temperature distribution is almost identical in shape to the field distribution shown in figure 11. Calculations have been made for forward half cycles with an extrapolated temperature distribution (essentially parabolic) and for the same constant temperature as the average of the distributed curve. The results of the calculations differed minimally. Previously,[3] similar results were obtained for reverse-bias calculations. Since the center of the diode heats faster than the ends during the forward conduction, and the ends heat faster during reverse conduction, the final temperature distribution should be fairly uniform if the forward power and reverse power are roughly equal.

[3] *A. L. Ward, Calculations of Second Breakdown in Silicon, Harry Diamond Laboratories, HDL-TR-1978 (August 1982).*

The rate of temperature rise for a given diode at a given applied voltage was found to be nearly independent of temperature for these calculations. The independence results from the opposing effects of higher breakdown voltage but lower current peaks as the temperature increases. Knowing the increase in temperature for both the forward and reverse single half cycles, one can readily approximate the total number of cycles to obtain any given temperature. Thus, the time to reach that temperature is found as a function of the impressed voltage amplitude.

Previous calculations[3] of single reverse-bias square pulses indicate that thermal second breakdown occurs at roughly 600 K. It is postulated that a negative resistance leads to current constriction and burnout. For an applied microwave pulse at the higher frequencies, the time required for current contraction may have a large effect. Two-dimensional calculations will be required to study this process.

8. CONCLUSION

Both forward and reverse characteristics have been calculated for microwave (half-cycle) voltage waveforms. The cutoff frequency for forward current flow has been shown to depend on diode width. The reverse current flow has been shown to be important above the diode breakdown voltage and to be sharply peaked in frequency. This shows that microwave burnout of diodes should be strongly frequency dependent at higher frequencies and short pulse lengths.

---

[3]*A. L. Ward, Calculations of Second Breakdown in Silicon, Harry Diamond Laboratories, HDL-TR-1978 (August 1982).*

LITERATURE CITED

(1) J. J. Whalen and H. Domingos, Square Pulse and RF Pulse Overstressing of UHF Transistors, Proceedings of the Electrical Overstress/Electrostatic Discharge Symposium, EOS-1 (1979), 140-146.

(2) J. H. Yee, W. J. Orvis, L. C. Martin, and J. C. Peterson, Modeling of Current and Thermal Mode Second Breakdown Phenomena, Proceedings of the Electrical Overstress/Electrostatic Discharge Symposium, EOS-4 (1982), 76-81.

(3) A. L. Ward, Calculations of Second Breakdown in Silicon, Harry Diamond Laboratories, HDL-TR-1978 (August 1982).

(4) A. L. Ward, Modes of Avalanche Oscillations in Silicon Diodes, IEEE Trans. Electron Devices, ED-25 (1978), 683-687.

(5) A. L. Ward, Oscillating Voltage Pulses and Second Breakdown, Proceedings of the Electrical Overstress/Electrostatic Discharge Symposium, EOS-2 (1980), 130-139.

(6) M. Caulton, A. Rosen, P. J. Stabile, and A. Gombar, p-i-n Diodes for Low-Frequency High-Power Switching Applications, IEEE Trans. Microwave Theory Tech., MTT-30 (1982), 875-882.

DISTRIBUTION

ADMINISTRATOR
DEFENSE TECHNICAL INFORMATION CENTER
ATTN DTIC-DDA (12 COPIES)
CAMERON STATION, BUILDING 5
ALEXANDRIA, VA 22314

COMMANDER
US ARMY MATERIEL COMMAND
ATTN MR. JAMES BENDER, AMCLD
5001 EISENHOWER AVE
ALEXANDRIA, VA 22333-0001

DEFENSE ADVANCED RESEARCH
PROJECT AGENCY
ATTN LTC RICHARD L. GULLICKSON, DEO
1400 WILSON BLVD
ARLINGTON, VA 22209

DEFENSE COMMUNICATIONS AGENCY
ATTN DR. PRAVIN JAIN
8TH STREET & SOUTH COURTHOUSE RD
ARLINGTON, VA 22204

DEFENSE INTELLIGENCE AGENCY
ATTN D. SPOHN, DB-4C2
ATTN DR. JAMES COLEMAN, DT-4C
ATTN CPT ROGER J. HOFFMAN, DC-7B
WASHINGTON, DC 20301

DIRECTOR
DEFENSE NUCLEAR AGENCY
ATTN CPT STONE, RAEE
ATTN GORDON SOPER
ATTN JACK MANSFIELD
WASHINGTON, DC 20305

INSTITUTE FOR DEFENSE ANALYSIS
ATTN DR. DEBORAH LEVIN
1801 N BEAUREGARD STREET
ALEXANDRIA, VA 22311

ASSISTANT TO THE SECRETARY OF DEFENSE
(ATOMIC ENERGY)
ATTN DR. RICHARD L. WAGNER
THE PENTAGON
ROOM 3E1074
WASHINGTON, DC 20301-3050

OFFICE OF THE UNDER SECRETARY OF DEFENSE
(RESEARCH & ENGINEERING)
ATTN ROBERT R. RANKINE, JR.
BRIGADIER GENERAL, USAF
THE PENTAGON
RM 3E1034
WASHINGTON, DC 20301-3050

COMMANDER
US ARMY ARMAMENT, MUNITIONS, & CHEMICAL
COMMAND
ATTN DRSMC-LEP-L, TECHNICAL LIBRARY

US ARMY ARMAMENT, MUNITIONS, & CHEMICAL
COMMAND (Cont'd)
ATTN DRSMC-ASF, FUZE & MUNITIONS
SUPPORT DIV
ROCK ISLAND, IL 61299

DIRECTOR
US ARMY BALLISTIC RESEARCH LABORATORY
ATTN DRDAR-TSB-S (STINFO)
ATTN DRSMC-BLV-R (A), J. McNEILLY
ATTN DRSMC-BLV-A (A), M. VOGEL
ABERDEEN PROVING GROUND, MD 21005

COMMANDER
US ARMY CAORA
ATTN ATOR-CAS-SO, MR. WALTERS
ATTN ATOR-CAS-SO, MR. HANSEN
FT LEAVENWORTH, KS 66027

US ARMY COMBINED ARMS CENTER
ATTN ATZL-CAM-D, A. T. BOWEN
FT LEAVENWORTH, KS 66027

COMMANDER
USA AIR DEFENSE SCHOOL
ATTN ATSA-CDM-W, CPT RAY GERTMAN
FT BLISS, TX 79916

US ARMY ELECTRONICS TECHNOLOGY &
DEVICES LABORATORY
ATTN DELET-MW, MR. WILSON,
EVANS AREA
ATTN DELET-DD
FT MONMOUTH, NJ 07703

COMMANDER
US ARMY ELECTRONIC WARFARE LABORATORY
OFFICE OF MISSILE ELECTRONIC WARFARE
ATTN DELEW-M-TAC, D. ALVAREZ,
A. K. PATTNI
WHITE SANDS MISSILE RANGE, NM 88002

COMMANDER
US ARMY FOREIGN SCIENCE
& TECHNOLOGY CENTER
ATTN DRXST-SD1, DR. T. A. CALDWELL
220 SEVENTH STREET, NE
CHARLOTTESVILLE, VA 22901

US ARMY MATERIEL SYSTEMS ANALYSIS AGENCY
ATTN DRXSY-CS, B. BRADLEY
ATTN DRXSY-GC, JAMES C. LIU
ABERDEEN PROVING GROUND, MD 21005-5071

DIRECTOR
US ARMY MATERIEL SYSTEMS ANALYSIS
ACTIVITY
ATTN DRXSY-MP
ABERDEEN PROVING GROUND, MD 21005

COMMANDER
US ARMY MISSILE COMMAND
ATTN DRSMI-RHB, H. GREENE
ATTN DRSMI-YSO, L. ALTGILBERS
REDSTONE ARSENAL, AL 35809

COMMANDER
US ARMY MISSILE & MUNITIONS
CENTER & SCHOOL
ATTN ATSK-CTD-F
REDSTONE ARSENAL, AL 35809

US ARMY MOBILITY EQUIPMENT RESEARCH &
DEVELOPMENT COMMAND
ATTN DRDME-E
ATTN DRDME-EC (2 COPIES)
ATTN DRDME-EA (2 COPIES)
ATTN DRDME-EM (2 COPIES)
ATTN DRDME-EE (2 COPIES)
ATTN DRCPM-MEP-D (2 COPIES)
ATTN DRCPM-MEP-M (2 COPIES)
ATTN DRCPM-MEP-T (2 COPIES)
ATTN ATZA-TSM-G (2 COPIES)
FT BELVOIR, VA 22060

COMMANDER
US ARMY RSCH & STD GP (EUR)
ATTN CHIEF, PHYSICS & MATH BRANCH
FPO NEW YORK 09510

US ARMY RESEARCH OFFICE
PO BOX 12211
ATTN DRXRO-PH, DR. B. D. GUENTHER
RESEARCH TRIANGLE PARK, NC 27709

COMMANDER
US ARMY TRAINING & DOCTRINE COMMAND
ATTN ATDO-TAG, WOLFORD
ATTN ATCD-M, GRAY
FT MONROE, VA 23651

DEPARTMENT OF THE ARMY
DEPUTY CHIEF OF STAFF, RDA
ATTN FRANK D. VERDERAME, DMAM-ARZ-D
WASHINGTON, DC 20310

HQ, AMC
ASSISTANT DEPUTY FOR SCIENCE & TECHNOLOGY
ATTN DR. R. L. HALEY, AMCDRA-ST
5001 EISENHOWER AVENUE
ALEXANDRIA, VA 22333-0001

INDUSTRIAL COLLEGE OF THE ARMED FORCES
ATTN ICFA-MSM, ROGER LEWIS
FT L. J. McNAIR
WASHINGTON, DC 20319

LETTERMAN ARMY INSTITUTE OF RESEARCH
ATTN SGRD-ULZ-IR, MAJ VANDRE
PRESIDIO OF SAN FRANCISCO, CA 94129

AIR FORCE WEAPONS LABORATORY
ATTN DR. BABU SINGARAJU, AFWL/NTC
ATTN MR. OTIS A. DAVENPORT, AFWL/NTC
KIRTLAND AFB, NM 87117

COMBAT DATA INFORMATION CENTER
AFWL-FIESD (CDIC)
WRIGHT-PATTERSON AFB, OH 45433

ROME AIR DEVELOPMENT CENTER
ATTN MR. RICHARD RABE, RADC/RBCM
GRIFFIS AFB, NY 13441

WRIGHT AERONAUTICAL LABORATORY
ATTN ROLAND D. VON ROHR, AAWW-1
ATTN DR. EDWIN B. CHAMPAGNE, AFWL/AAD
WRIGHT-PATTERSON AFB, OH 45433

HQ, USAF
DEPARTMENT OF THE AIR FORCE
ATTN MAJ CLARENCE M. BOSE, INYX
WASHINGTON, DC 20330

US AIR FORCE TECHNICAL
ASSESSMENT CENTER
ATTN CPT ROSS L. AMICO, TAO
PATRICK AFB, FL 32925

HQ, USAF/SAMI
WASHINGTON, DC 20330

RELIABILITY ANALYSIS CENTER
RADC (RBRAC)
ATTN DATA COORDINATOR/GOVT PROGRAMS
GRIFFISS AFB, NY 13441

HQ
AIR FORCE ELECTRONIC WARFARE
CENTER (ESC)
ATTN SAXA, J. GIORLANDO
SAN ANTONIO, TX 78243

HEADQUARTERS, AIR FORCE SYSTEMS
COMMAND
ATTN DLWM, CPT JUDITH COOK
ANDREWS AFB, MD 20334

USAFSAM/RZP
ATTN DAVID N. ERWIN
BROOKS AFB, TX 78235

AFWAL/AADM
ATTN DONALD REES
WRIGHT-PATTERSON AFB, OH 45433

AFWL
ATTN LTC GENEROSA, NTYD
ATTN MAJ ABRAM F. JACK, NTYN
KIRTLAND AFB, NM 87117

NAVAL INTELLIGENCE SUPPORT
CENTER
ATTN ARTHUR G. COBLEIGH, JR., NISC-51
ATTN MR. ALBERT LEAVITT
4201 SUITLAND ROAD
WASHINGTON, DC 20390

NAVAL RESEARCH LABORATORY
ATTN MOSHE FRIEDMAN, CO 4700.1
ATTN SIDNEY L. OSSAKOW, CO 4700
ATTN T. J. WIETING, CO 6652
4555 OVERLOOK AVENUE, SW
WASHINGTON, DC 20376

NAVAL SEA SYSTEMS COMMAND
ATTN GEORGE M. BATES
PMS-405-300
WASHINGTON, DC 20362

COMMANDER
NAVAL SURFACE WEAPONS CENTER
ATTN DR. VINCENT PUGLIELLI, R. RICHARDSON
DAHLGREN, VA 22448

ANALYTICAL SYSTEMS ENGINEERING CORP
OLD CONCORD ROAD
ATTN LIBRARIAN
BURLINGTON, MA 01803

ARNOLD ENGINEERING DEVELOPMENT
CENTER
ATTN LARRY CHRISTENSEN
MAIL STOP 640
TULLAHOMA, TN 37388

AAI CORPORATION
PO BOX 6767
RECORDS DEPARTMENT
BALTIMORE, MD 21204

THE AEROSPACE CORPORATION
PO BOX 92957
ATTN N. S. MAS, M4/928
LOS ANGELES, CA 90009

BERKELEY RESEARCH ASSOCIATES
PO BOX 852
ATTN DR. E. C. ALCARAZ
SPRINGFIELD, VA 22150

THE BDM CORPORATION
ATTN MR. IGOR D. GERHARDT
2227 DRAKE AVENUE
SUITE 25
HUNTSVILLE, AL 35805

BOEING MILITARY AIRPLANE COMPANY
ATTN CLETUS SUTTER
M/S: K75-50
3801 SOUTH OLIVER
WICHITA, KS 67210

BOEING AEROSPACE COMPANY
PO BOX 3707
ATTN D. W. EGELKROUT, MS 2R 00
SEATTLE, WA 98124

BOEING AEROSPACE COMPANY
PO BOX 3999
ATTN DR. ERVIN J. NALOS, 2-3741-EJN-288
SEATTLE, WA 98124

DIRECTED TECHNOLOGIES, INC
ATTN MR. IRA F. KUHN, JR.
1226 POTOMAC SCHOOL ROAD
McLEAN, VA 22101

DIRECTOR
NATIONAL SECURITY AGENCY
ATTN MS GAIL J. REINHEIMER, A4
FT MEADE, MD 20755

EOS TECHNOLOGIES, INC
ATTN DR. R. E. LeLEVIER
606 WILSHIRE BLVD
SUITE 700
SANTA MONICA, CA 90401

ENGINEERING SOCIETIES LIBRARY
ATTN ACQUISITIONS DEPARTMENT
345 EAST 47TH STREET
NEW YORK, NY 10017

GENERAL DYNAMICS/POMONA DIVISION
ATTN DR. K. H. BROWN, MZ 401-10
ATTN DIVISION LIBRARY, 4-20
ATTN MR. HAME, MZ 401-11
POMONA, CA 91769

GRUMMAN AEROSPACE CORPORATION
ATTN A. G. ZIMBALATTI
BETHPAGE, NY 11714

R. C. HANSEN, INC
PO BOX 215
ATTN R. C. HANSEN
TARZANA, CA 91356

IRT CORPORATION
ATTN HAROLD T. BUSCHER
3030 CALLAN ROAD
SAN DIEGO, CA 92121

IRT CORPORATION
PO BOX 85317
ATTN DR. FRANK CHILTON
SAN DIEGO, CA 92138

KAMAN SCIENCES CORPORATION
PO BOX 7463
ATTN J. LAMAR ALLEN
ATTN THOMAS A. TUMOLILLO

KAMAN SCIENCES CORPORATION (Cont'd)
ATTN RICHARD A. WALLNER
COLORADO SPRINGS, CO 80933

KAMAN SCIENCES CORPORATION
ATTN EDWARD E. CONRAD, DOC CONT
ATTN SUITE 1200
1911 JEFFERSON DAVIS HIGHWAY
ARLINGTON, VA 22202

DASIAC-DETIR
KAMAN TEMPO
ATTN MR. F. WIMENITZ
2560 HUNTINGTON AVENUE, SUITE 500
ALEXANDRIA, VA 22303

KAMAN TEMPO
ATTN D. REITZ
816 STATE STREET
(PO DRAWER QQ)
SANTA BARBARA, CA 93102

LAWRENCE LIVERMORE NATIONAL
LABORATORY
PO BOX 808
ATTN MR. BLAND, L-153
ATTN HRIAR S. CABAYAN, L-313
ATTN J. B. CHASE, L-313
ATTN T. R. KONCHER, L-389
ATTN GEORGE H. MILLER, L-13
ATTN W. J. SHOTS, L-23
ATTN WALTER R. SOOY, L-488
LIVERMORE, CA 94550

LOCKHEED MISSILES & SPACE
COMPANY, INC
ATTN JOHN G. SIAMBIS
ATTN CHARLES J. TRIANGALI
3251 HANOVER STREET
PALO ALTO, CA 94304

LOS ALAMOS NATIONAL LAB
PO BOX 1663 MS-5000
ATTN R. S. DINGUS
ATTN ROBERT F. HOBERLING
ATTN JEREMY A. LANDT
ATTN FREDERICK A. MORSE
ATTN J. W. TAYLOR
ATTN L. B. WARNER
LOS ALAMOS, NM 87545

MARTIN MARIETTA ORLANDO
AEROSPACE
PO BOX 5837, MP 480
ATTN DR. B. L. CLARK
ATTN MR. CHARLES R. CRANFORT
SAND LAKE ROAD
ORLANDO, FL 32855

MAXWELL LABORATORIES, INC
ATTN F. MARC de PIOLENC
8835 BALBOA AVENUE
SAN DIEGO, CA 92123

McDONNELL DOUGLAS CORPORATION
McDONNELL DOUGLAS RESEARCH LAB
PO BOX 516
ATTN D. P. AMES,
DEPT. H220, BLDG. 110
ST LOUIS, MO 63166

MISSION RESEARCH CORPORATION
PO BOX 279
ATTN MS. DAWN HIGGS
SPRINGFIELD, VA 22150

THE MITRE CORPORATION
TECHNICAL REPORT CENTER
ATTN DR. J. R. VAN ZANDT, H-060
BURLINGTON ROAD
BEDFORD, MA 01730

PACIFIC-SIERRA RESEARCH CORPORATION
ATTN LEONARD SCHLESSINGER
12340 SANTA MONICA BLVD
LOS ANGELES, CA 90025

PHYSICS INTERNATIONAL
ATTN EMIL KOVTUN, J. BENFORD
ATTN ALAN J. TOEPFER
2700 MERCED STREET
SAN LEANDRO, CA 94577

PULSE SCIENCES INC
ATTN PHILIP D'A. CHAMPNEY
14796 WICKS BLVD
SAN LEANDRO, CA 94577

QUEST RESEARCH CORPORATION
ATTN ROBERT S. OHANESIAN
6858 OLD DOMINION DRIVE
McLEAN, VA 22101

RAND
ATTN ALEXANDER F. BREWER
1700 MAIN STREET
SANTA MONICA, CA 90406

R&D ASSOCIATES
PO BOX 9695
ATTN MR. B. MOLLER
MARINA DEL RAY, CA 90291

SAFSS
ATTN LTC MARK HODGESON
WASHINGTON, DC 20330

DISTRIBUTION (Cont'd)

SANDIA NATIONAL LAB
PO BOX 969 DIV. 8341
ATTN MURRAY S. DAW
LIVERMORE, CA 94550

SANDIA NATIONAL LAB
PO BOX 5800
ATTN CHARLIE R. BLAINE
ATTN KENNETH R. PRESTWICH
ATTN MAX B. SANDOVAL
ALBUQUERQUE, NM 87185

SCIENCE APPLICATIONS, INC
ATTN LINDA WHITMEYER
1215 JEFFERSON DAVIS HIGHWAY
SUITE 310
ARLINGTON, VA 22202

SCIENCE APPLICATIONS, INC
ATTN DR. EDWARD CORNET
ATTN DR. ADAM T. DROBOT,
DIV. 157
1710 GOODRIDGE DRIVE
McLEAN, VA 22102

SCIENCE APPLICATIONS, INC
ATTN CHARLES L. YEE
#5 PALO ALTO SQUARE, SUITE 200
PALO ALTO, CA 94306

W. J. SCHAFER ASSOCIATES, INC
ATTN DOCUMENT CONTROL
1901 N. FT MYER DR.
SUITE 800
ARLINGTON, VA 22209

W. J. SCHAFER ASSOCIATES, INC
CORPORATE PLACE 128
BUILDING 2, SUITE 300
ATTN DR. JAMES P. REILLY
WAKEFIELD, MA 01880

SYRACUSE RESEARCH CORPORATION
ATTN DR. D. T. AUCKLAND
MERRILL LANE
SYRACUSE, NY 13210

SRI, INC
ATTN DR. GERALD AUGUST,
ELECTROMAGNETIC SCIENCES
LABORATORY
333 RAVENSWOOD AVENUE
MENLO PARK, CA 94025

TITAN SYSTEMS, INC
ATTN DOCUMENT CONTROL, LB
9191 TOWNE CENTRE DRIVE, SUITE 500
SAN DIEGO, CA 92122

TRW DEFENSE SYSTEMS GROUP
ATTN PRAVIN G. BHUTA,
MS 132/9085
ATTN E. V. RUTKOWSKI,
81/1526
ONE SPACE PARK DRIVE
REDONDO BEACH, CA 90278

TRW SPACE & TECHNOLOGY GROUP
DIRECTED ENERGY LABORATORY
ATTN DR. ZAVEN G. GUIRAGOSSIAN
ONE SPACE PARK
REDONDO BEACH, CA 90278

VARIAN ELECTRON DEVICE GROUP
ATTN MR. IRV MALTZER, E-419
611 HANSEN WAY
PALO ALTO, CA 94303

US ARMY ELECTRONICS RESEARCH &
DEVELOPMENT COMMAND
ATTN COMMANDER, AMDEL-CG
ATTN TECHNICAL DIRECTOR, AMDEL-CT
ATTN PUBLIC AFFAIRS OFFICE, AMDEL-IN

HARRY DIAMOND LABORATORIES
ATTN D/TSO/DIVISION DIRECTORS
ATTN RECORD COPY, 81200
ATTN HDL LIBRARY, 81100 (3 COPIES)
ATTN HDL LIBRARY, 81100 (WOODBRIDGE)
ATTN TECHNICAL REPORTS BRANCH, 81300
ATTN LEGAL OFFICE, 97000
ATTN ZABLUDOWSKI, B., 47400 (GIDEP)
ATTN CHIEF, 21000
ATTN CHIEF, 21100
ATTN CHIEF, 21200
ATTN CHIEF, 21300
ATTN CHIEF, 21400
ATTN CHIEF, 21500
ATTN CHIEF, 22000
ATTN CHIEF, 22100
ATTN CHIEF, 22300
ATTN CHIEF, 22800
ATTN CHIEF, 22900
ATTN CHIEF, 20240
ATTN CHIEF, 11100
ATTN SILVERSTEIN, J., 13300
ATTN R. GARVER, 21100 (4 COPIES)
ATTN E. BROWN, 00211
ATTN J. BOMBARDT, 00100
ATTN J. MICHALOWICZ, 22100
ATTN G. V. CIRCINCIONE, 22300
ATTN J. SCZEPANSKI/R. CLAFFY, DRXCM-RC
ATTN F. AGEE/S. GRAYBILL, 22900
ATTN S. SHARE, 22100
ATTN A. STEWART, 20240
ATTN H. DROPKIN, 13200
ATTN A. WARD, 21100 (20 COPIES)

END

FILMED

12-84

DTIC